Generalized Bernoulli Gauss von Mises Distribution for Uncertainty Realism on Saddle-Center Spaces

Ryne Beeson
Mechanical and Aerospace Engineering
Princeton University
Princeton, New Jersey, USA
ryne@princeton.edu

***Abstract*—Most aspects of space situational awareness (SSA) rely on accurate and efficient uncertainty realism, propagation, and nonlinear filtering. A new frontier for SSA is the application to the cislunar realm, which lacks a global orbital element coordinate set. The dynamics of a representative model, the circular restricted three-body problem (CR3BP), for the cislunar domain provides the opportunity to define local orbital elements using dynamical systems techniques such as normal form theory. Motivated the structure of the CR3BP SSA problem, we construct a generalized Bernoulli Gauss von Mises distribution, that is defined on local orbit element coordinates generated from normal form theory at a saddle-center-center equilibrium point, and show its ability to capture what may be a common deformation mode of the CR3BP.**

I. Introduction

The operations and decision making processes of space situational awareness (SSA) are reliant on the certainty of knowing a space object (SO) state at a given sequence of times in a specified coordinate system. Updating the uncertainty is accomplished through estimation, which in the case of discrete-time observations, involves two steps; the first involving propagation of the initial uncertainty to the prior distribution, and the second involving the update to the posterior distribution given new observations (e.g., radar measurements, electro-optical images, etc.). In this paper, we focus on the improvement of the first step of this process, uncertainty realism and propagation, for systems that have saddle-center type equilibria. Our motivation arises from the near future need to extend the SSA mission from the Earth-bound realm to the greater cislunar lunar domain, and that fact that the cislunar domain approximated by the circular restricted three-body problem (CR3BP) possess this saddle-center structure. Because this dynamical structure is modeled as a product of singular and cylinder spaces, and because we can approximate the dynamics on this manifold as linear, we construct a new distribution, the generalized Bernoulli Gauss von Mises that is naturally adapted to the manifold space and evolves in a predictable manner.

We begin this paper in §II by motivating the use of well chosen coordinate systems and the use of directional statistics for modeling distributions for SSA on a cylinder space. In §III we introduce the dynamical structure of the CR3BP, the main steps of the normal form application and creation of the local orbital elements. We then describe the construction of the new distribution in §IV.

II. Uncertainty Realism and Propagation in the Two-Body Problem

The position and velocity state of a SO under perturbed relative two-body dynamics, expressed in a cartesian coordinate system, evolves according to,

$$\ddot{r} = -\frac{\mu_\oplus}{|r|^3} r + f(r, \dot{r}, t), \quad r, \dot{r} \in \mathbb{R}^3, \tag{II.1}$$

where $|\cdot|$ is the l_2-norm, $\mu_\oplus$ the gravitational constant of the central gravitational body and f represents disturbing acceleration forces (e.g., aspherical gravitational potential, third-body forces, solar radiation pressure, atmospheric drag, etc.). As is the case in many uncertainty propagation and nonlinear filtering scenarios, it is desirable to model (if realistic) the uncertainty distribution associated with a state as a multivariate Gaussian. Even though the dynamics given by Eq. II.1 are sufficiently simple, they are nonlinear. As we demonstrate in an example problem of §II-A1, a reasonable Gaussian uncertainty develops a highly non-Gaussian *boomerang* shape after only a few orbital periods.

From this starting observation, there are two reasonable approaches to improving the uncertainty realism and propagation (UR&P). The first involves finding a new coordinate system upon which the dynamics of the SO are less nonlinear and therefore a Gaussian will propagate to a Gaussian. In this case, our modeling can build around Gaussian properties more directly. The second approach accepts the nonlinear dynamics and attempts to improve UR&P with adaptive, mixture, or other functional representative techniques. We illustrate the ideas of the first approach starting in §II-A and then more deeply in §III where this becomes the main line of thought for developing a distribution naturally on a saddle-center space. We briefly provide relevant background literature on the second approach for SSA in §II-B, which will further enhance the approach of this paper moving forward.

A. (Equinoctial) Orbital Elements

Orbital element sets for the relative two-body problem provide a geometric coordinate system to describe the state of the SO. They also decompose the dynamics into fast and

slow components. The slow elements generally have constant values for the unperturbed relative two-body problem. The Keplerian (classical) elements $(a, e, i, \Omega, \omega, \nu)$ are the best known set and consist of five slow (constant in the unperturbed case) variables: a the semi-major axis, e the eccentricity, i the inclination, Ω the longitude of the ascending nodes, and ω the argument of periapsis; with one fast angular variable: ν the true anomaly. Another useful element set is the equinoctial orbital elements that remove singularities of the Keplerian elements (zero eccentricity or inclination), but more importantly for this paper, reduce the angular variable to one that varies linearly in time with all other elements constant (the unperturbed case). Hence the natural manifold for the equinoctial elements is $\mathbb{R}^5 \times S^1$, which we will also refer to as a cylinder space. S^1 is the unit circle and is the domain for an angular coordinate. The following example demonstrates the *boomerang* behavior previously described, and illustrates the type of deformation that must be captured for UR&P, regardless of whether cartesian or cylinder coordinates are used.

1) Motivational Two-Body Example: Horwood and Poore [1] put forth the following example problem to demonstrate the *boomerang* effect. Consider a SO with osculating equinoctial orbital elements at an initial epoch given by,

$$(a, h, k, p, q, l) = (7136.635 \text{ km}, 0, 0, 0, 0, 0 \text{ rad}). \quad \text{(II.2)}$$

This is a circular, zero-inclination orbit at Earth with an altitude of 765 km. Assume that the initial uncertainty is given by a 6-dimensional Gaussian with covariance,

$$P = \text{diag}((20 \text{ km})^2, 10^{-6}, 10^{-6}, 10^{-6}, 10^{-6}, \kappa^{-1} \text{ rad}^2),$$

where diag is a diagonal matrix and $\kappa = 3.282806 \cdot 10^7$.

A Monte Carlo (MC) sampling of this Gaussian at the initial epoch is performed and advected under two-body dynamics with a perturbing force from an 8×8 Earth aspherical gravitational potential for four orbital periods. The result is shown in Fig. 1, where we also display the uncertainty propagation of an Extended Kalman Filter (EKF) (i.e., propagation of the covariance under the linearized dynamics) and the Unscented Transform (UT). Samples from a distribution constructed on the cylinder space by Horwood and Poore, the Gauss von Mises (GvM) distribution that will be introduced in §II-D, are also shown. Clearly, the variance inflation of the UT is excessive and the EKF has collapsed, while the GvM is able to accurately capture the *boomerang* shape.

B. General Approaches

1) Gaussian Statistics and Higher Order Taylor Series Expansions: One can go beyond propagation of the covariance under linearized dynamics, by considering higher order Taylor series expansions. The obvious drawbacks of this approach are the derivation of the higher order derivatives, a higher dimensional state to be advected, and possibly little gained in terms of the convergence radius. Park and Scheeres [2] developed an *intrusive* method using higher order Taylor series expansions. Their approach was further extended in Fujimoto and Scheeres [3] and Roa and Park [4].

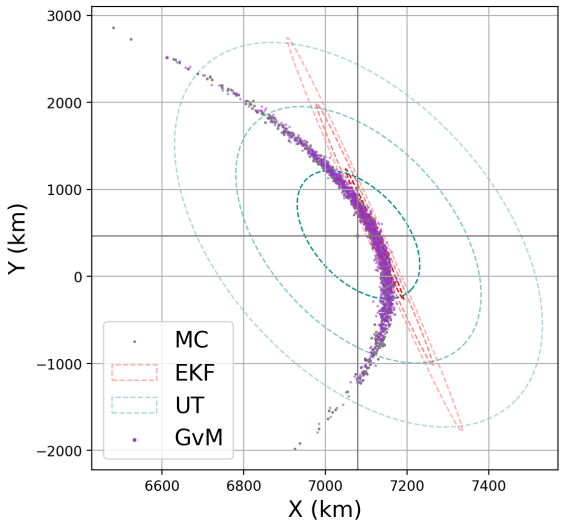

Fig. 1: Advection of the samples after four orbits

2) Unscented Transform: A standard approach to improve over the linearized dynamics of the EKF is by advecting particles under the full nonlinear dynamics and then reconstructing statistics based on these advected particles. In a series of papers by Julier et al. [5], Julier [6], and Julier and Uhlmann [7] the unscented transform was introduced to approximate nonlinear mapping of Gaussian distributions using Gauss-Hermite weighted quadrature rules that could exactly integrate polynomials of specific order.

3) Gaussian Mixture Models (GMM): GMMs were introduced for recursive Bayesian estimation by Sorenson and Alspach [8, 9]. They provide a flexible way to approximate a non-Gaussian, but require a method to fit the mixture to the desired distribution and still suffer uncertainty realism issues over long time periods or under chaotic dynamics. Terejanu et al. [10], DeMars and Jah [11], and DeMars et al. [12] have all contributed impactful papers in this area.

4) Polynomial Chaos Expansion (PCE): The GMM approach can be thought of as a local method of low order, whereas the PCE is a spectral approach with global support. Jones et al. [13] have applied a (non-intrusive) PCE [14] approach to perform SSA uncertainty quantification.

5) Hybrid Approaches: Approaches that combine the GMM and PCE approach have been explored by Vittaldev et al. [15]. Wan and Karniadakis [16] have developed multi-element generalized PCE methods.

C. von Mises Distribution

Orbital elements can naturally be viewed as evolving on $\mathbb{R}^5 \times S^1$, and Fig. 1 also makes clear that modeling the fast angular component on a unit circle should be more efficient and accurate. There are a number of distributions defined on the unit circle that approximate a Gaussian on $\mathbb{R}$. The *wrapped normal distribution* is defined by evaluating the normal distribution on $\mathbb{R}$ under an infinite summation after partitioning $\mathbb{R}$ by intervals of 2π length. The von Mises

distribution [17] provides a close approximate while avoiding the infinite summation,

$$\mathcal{VM}(\theta;\alpha,\kappa) = \frac{1}{2\pi e^{-\kappa} I_0(\kappa)} e^{-2\kappa \sin^2 \frac{1}{2}(\theta-\alpha)}.$$

D. Gauss von Mises Distribution

The first to construct and use a circular distribution for the purposes of UR&P was Horwood and Poore with a series of works [18, 1, 19]. They constructed a distribution on $\mathbb{R}^5 \times S^1$ for representation of uncertainty of equinoctial orbital elements. The distribution is a product of a Gaussian distribution on $\mathbb{R}^5$ with a von Mises distribution on S^1 and a specific correlation structure between the two distributions such that the boomerang type deformation encountered in the two-body problem can be approximated. This new distribution was named the *Gauss von Mises* $\mathcal{GVM}$ distribution and has the following definition,

$$\begin{aligned}\mathcal{GVM}(x,\theta;\mu,P,\alpha,\beta,\Gamma,\kappa)\\ \equiv \mathcal{N}(x;\mu,P)\mathcal{VM}(\theta;\Theta(x;\mu,P,\alpha,\beta,\Gamma),\kappa),\end{aligned}$$

where

$$\mathcal{N}(x;\mu,P) = \frac{1}{\sqrt{\det(2\pi P)}} \exp\left(-\frac{1}{2}\langle x-\mu, P^{-1}(x-\mu)\rangle\right),$$

and

$$\begin{aligned}&\mathcal{VM}(\theta;\Theta(x;\mu,P,\alpha,\beta,\Gamma),\kappa)\\ &= \frac{1}{2\pi e^{-\kappa} I_0(\kappa)} \exp\left(-2\kappa \sin^2(\frac{1}{2}(\theta-\Theta(x)))\right). \quad \text{(II.3)}\end{aligned}$$

Correlation is controlled by the conditional mean,

$$\begin{aligned}\Theta(x) &\equiv \alpha + \langle \beta, z\rangle + \frac{1}{2}\langle z, \Gamma z\rangle,\\ z &= A^{-1}(x-\mu), \qquad P = AA^T,\end{aligned} \quad \text{(II.4)}$$

$\alpha \in S^1$, $\beta \in \mathbb{R}^5$, $\Gamma \in \mathbb{R}^{5\times 5}$ is a symmetric matrix, A is the Cholesky factor of P, and $(x,\theta) \in \mathbb{R}^5 \times S^1$ (e.g., equinoctial orbital elements). The key to the construction of the $\mathcal{GVM}$ is the choice of $\Theta(x)$. Intuitively, α provides the standard concentration location as in the univariate $\mathcal{VM}$, the β parameter allows for linear correlation, and Γ provides a quadratic correlation that is meant to help capture the boomerang feature. When β and Γ are both equal to zero (vectors and matrices), then the Gaussian and von Mises distributions are independent. Elementary properties of the $\mathcal{GVM}$ distribution are given in Horwood and Poore [1] including a routine for propagation and refitting of the $\mathcal{GVM}$, which allows us to achieve the sampling shown in Fig. 1. We recall this propagation routine here for the purposes of more clearly aligning our work in §IV.

1) Propagation Routine: If the $\mathcal{GVM}$ distribution is a good distribution for the UR&P problem at hand, then given an initial $\mathcal{GVM}$ distribution at the epoch $t = 0$, we should be able to find a family of distributions $(\mathcal{GVM}_t)_{t\in[0,T]}$ over the time interval $[0,T]$ with $T > 0$, under the dynamical flow map φ that well approximate the true uncertainty evolution. Because the $\mathcal{GVM}$ is defined by the parameters, $(\mu, P, \alpha, \beta, \Gamma, \kappa)$, the real task is to evolve these parameters or refit these parameters at a future time. This is the goal of the propagation routine; for example:

1) Based on deterministic quadrature rules draw quadrature nodes $(X_i)_{i=1}^N$ from the $\mathcal{GVM}_0$ and assign appropriate weights $(w_i)_{i=1}^N$. Denote the parameters of $\mathcal{GVM}_0$ as,
$$Z_0 = (\mu_0, P_0, \alpha_0, \beta_0, \Gamma_0).$$
2) Advect the nodes to the desired time t and generate estimates of the $\mathcal{GVM}_t$ parameters $Z_t = (\mu_t, P_t, \alpha_t, \beta_t, \Gamma_t)$ based on the weighted ensemble; let us denote these estimates as,
$$\widetilde{Z}_t = (\widetilde{\mu}_t, \widetilde{P}_t, \widetilde{\alpha}_t, \widetilde{\beta}_t, \widetilde{\Gamma}_t).$$
3) Formulate an optimization problem with the intent to improve the parameter estimates $\widetilde{Z}$ such that the statistical significance of the samples $((w,X)_i)$ at the initial time is nearly that at the final time t. For this purpose, the squared difference of the Mahalanobis von Mises statistic given below in Eq. II.6 is convenient,
$$J(\widetilde{Z}) = \sum_{i=1}^{N} \left(M(X_i;Z_0) - M(\varphi_t(X_i);\widetilde{Z})\right)^2. \quad \text{(II.5)}$$

2) Mahalanobis von Mises Statistic: The Mahalanobis statistic for a multivariate Gaussian random variable, provides a distance by which to discern the statistically significance of a given sample. The Mahalanobis von Mises statistic has a similar meaning and is given by,

$$\begin{aligned}M(x,\theta;\mu,P,\alpha,\beta,\Gamma,\kappa) \equiv \langle x-\mu, P^{-1}(x-\mu)\rangle\\ + 4\kappa \sin^2\left(\frac{1}{2}(\theta-\Theta(x))\right), \quad \text{(II.6)}\end{aligned}$$

for $(x,\theta) \sim \mathcal{GVM}(\mu,P,\alpha,\beta,\Gamma,\kappa)$.

It is informative to compare the robustness and stability of the $\mathcal{GVM}$ to a more general approach, such as a GMM. Consider a similar problem setup as before, where the initial orbital reference state is given by classical orbital elements,

$$(a,e,i,\Omega,\omega,\nu) = (7071 \text{ km}, 0.01, 0.01, 0.01, 0.01, 0.),$$

and we assume an initial position variance of 10 km^2 in each cartesian component and 1 m^2 / s^2 in each cartesian velocity component. In Fig. 2 we compare the normalized Mahalanobis statistic for an EKF, UT, GMM (with 15 components optimized using the approach in [20]), and the Mahalanobis von Mises statistic for the GvM against 50 MC samples over a 5 orbital period (1 TU is 1 orbital period in the figure). The normalization factor is shown in the legend and this approach is taken to better illustrate the relative variability of each method over the propagation window. What is clear is that the GvM (given by pink lines) is nearly constant over the 5 orbital periods for each MC sample, whereas the GMM has small but frequent oscillations, the UT has large and quickly varying oscillations, and this is even worse for the EKF. For

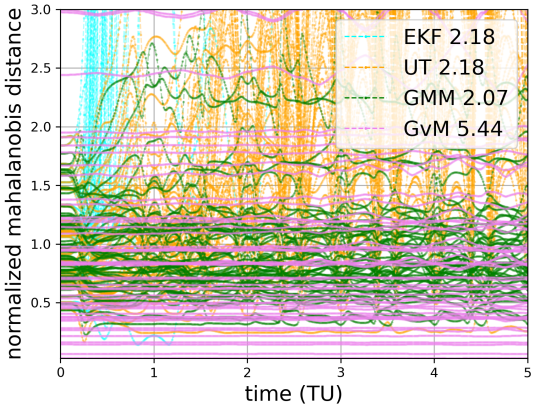

Fig. 2: Normalized Mahalanobis (von Mises) statistic over propagation time for the unperturbed two-body problem of §II-D2 for 50 MC samples.

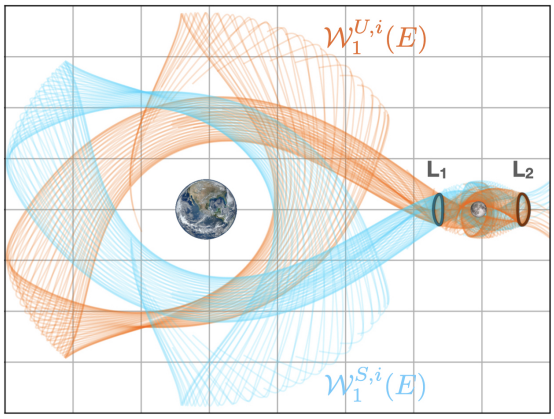

Fig. 3: Depiction of the Earth-Moon CR3BP with the libration points L_1 and L_2 identified, as well as stable (e.g., $\mathcal{W}_1^{S,i}(E)$) and unstable (e.g., $\mathcal{W}_1^{U,i}(E)$) invariant manifolds to Lyapunov orbits (generated in **pydylan** [22]).

additional remarks and observations on the construction and performance of the $\mathcal{GVM}$, as well as a discussion of other directional statistics models that should be explored to extend the $\mathcal{GVM}$ on the two-dimensional problem, see Beeson [21].

III. Cislunar Dynamics, Normal Form Theory, and Local Orbital Elements

The simplest dynamical model to represent the dynamics of the Earth-Moon cislunar realm is the CR3BP. It is a relative model for the SO dynamics with respect to a synodic rotating frame placed at the barycenter of the two primaries, which are assumed to follow circular orbits about the barycenter. The model is cast in non-dimensional units, with a new gravitational parameter μ (approximately 1.215E-2 for Earth-Moon), and the unit distance being the constant distance between the two primaries. Of great importance is the existence of five libration points (relative equilibria). We provide a depiction of the location of the L_1 and L_2 libration points in Fig. 3.

The CR3BP is a Hamiltonian system with a rich dynamical structure. The collinear libration points are of saddle-center-center type, possessing stable-unstable directions, and possess nearby periodic orbits that can be continued in the region of the libration points; these contain the Lyapunov, Halo, and Lissajous families. These periodic orbits have their own invariant manifolds, a few of which are also shown in Fig. 3 that act to separate the dynamical flow and result in the chaotic behavior of the CR3BP.

A. Cislunar Motivational Problem

The instability at these periodic orbits and libration points require new techniques for reliable UR&P in the cislunar realm, where observations may not be as frequent, nor of such high information content as that typical of Earth-bound SO. Let us illustrate this remark via an example borrowed from Chow II et al. [23]. Consider a planar L_1 Lyapunov orbit like that shown in Fig. 3, and which possesses a Jacobi energy of approximately 3.168 The initial uncertainty is assumed to be Gaussian with a position and velocity variance of 10 km^2 and 1 m^2 / second^2 in each coordinate direction respectively. The orbital period of this Lyapunov is slightly more than 12 days and we consider a propagation time of 7 days. An initial Monte Carlo sampling is performed and the final values are shown in Fig. 4.

B. Normal Form Theory

Motivated by the boomerang deformation mode shown in Fig. 4 we aim to leverage the effectiveness of a construct like the $\mathcal{GVM}$ for the two-body problem. This requires that we construct a coordinate system for the problem of §III-A whereby the evolution is viewed on a cylinder or spherical space with the angular component correlated to fixed or very slowly evolving states. For Hamiltonian systems, a natural way to construct such a coordinate system is to apply the normal form theory (c.f., Meyer and Offin [24] or Wiggins [25] for general dynamical systems). The outcome of applying this theory to an equilibrium point, which is what we perform here, is a series of nonlinear transformations to reduce the dynamics in a neighborhood about the equilibrium point into their simplest form,

$$(x, \dot{x}, y, \dot{y}, z, \dot{z}) \to (I_1, \varphi_1, I_2, \varphi_2, I_3, \varphi_3),$$

where the new *action* coordinates I_j are constant and the *angle* coordinates φ_j evolve linearly with respect to time. We provide a very brief summary here of the main steps to achieve this for our motivating problem and otherwise point the reader to [24, 25, 26] for general theory and to Jorba [27] for an efficient numerical approach by which these techniques can be implemented.

Expressed in position (x, y, z) and momenta (p_x, p_y, p_z) coordinates, the Hamiltonian of the CR3BP is given by,

$$H(x, p_x, y, p_y, z, p_z) = \frac{1}{2}|p|^2 + yp_x - xp_y - \frac{1-\mu}{r_1} - \frac{\mu}{r_2},$$
$$r_1^2 = (x-\mu)^2 + y^2 + z^2, \quad r_2^2 = (x-\mu+1)^2 + y^2 + z^2.$$

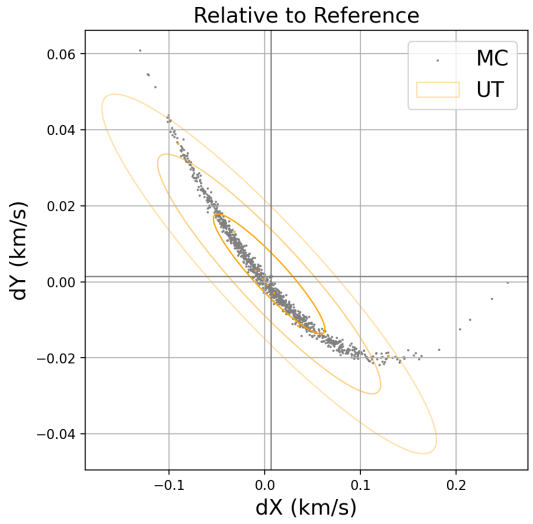

Fig. 4: Evolution of MC samples from an initial Gaussian uncertainty distribution discussed in §III-A after 7 days in the CR3BP dynamics.

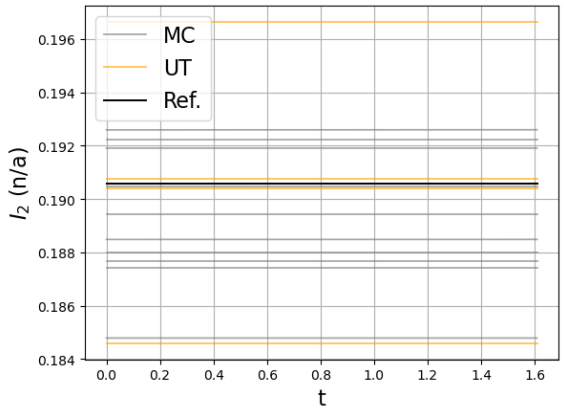

Fig. 5: Evolution of the action variable for a center term of UT nodes, MC samples, and Lyapunov orbit. Time units are non-dimensionalized, final time equivalent to 7 days.

To apply normal form theory requires our Hamiltonian to be of the form,

$$H(x, p_x, y, p_y, z, p_z) = \sum_{|n|\geqslant 2} H_n(x, p_x, y, p_y, z, p_z), \quad \text{(III.1)}$$

where H_n is a homogeneous polynomial of order $|n|$, where $n \in \mathbb{N}_0^6$ is a multiindex for the powers of the components $\xi \equiv (x, p_x, y, p_y, z, p_z)$, and $|n| \equiv \sum_{i=1}^{6} n_i$. This can be achieved with the help of Legendre polynomials for the CR3BP. After translating the coordinate system to the equilibrium point of interest and coordinate transformation based on the linearized dynamics of the equilibrium point, given by H_2, is performed. This decomposes the configuration space into the saddle (stable-unstable) and center subspaces.

The main steps of the normal form then proceed by a series of Lie transformations (here using the Poisson bracket definition) used to transform $H \to H'$,

$$H' = H + \{H, G\} + \frac{1}{2!}\{\{H, G\}, G\} + \cdots, \quad \text{(III.2)}$$

where G is a *generating function* and $\{\cdot, \cdot\}$ is the Poisson bracket,

$$\{f, g\} = \sum_{i=1}^{3} \frac{\partial f}{\partial q_i}\frac{\partial g}{\partial p_i} - \frac{\partial f}{\partial p_i}\frac{\partial g}{\partial q_i} = \langle \nabla f, J\nabla g\rangle,$$

where J is the (canonical) symplectic matrix. The generating functions $(G_j)_{j=1}^{N}$ to order $N \in \mathbb{N}$ can be computed simply from the coefficients of the monomials of Eq. III.1 (or Eq. III.2 as we recursively transform), the multiindices of the monomials, and knowledge of the linearized dynamics given by H_2. The final step of the normal form is to identify new coordinates with the saddle and center subspaces, which result in an integrable Hamiltonian of order N once higher order terms are dropped[1].

In this work we identify the (I_1, φ_1) pair with a saddle manifold and (I_2, φ_2) and (I_3, φ_3) with center manifolds. The domain of each of these is,

$$\begin{aligned} &I_1 \in \mathbb{R}, \quad \varphi_1 \in \mathbb{C}, \\ &I_j \in \mathbb{R}_+ \cup \{0\} = \overline{\mathbb{R}}_+, \quad \varphi_j \in S^1, \quad j \in \{2, 3\}, \end{aligned} \quad \text{(III.3)}$$

but in particular the real and complex parts of φ_1 takes one of the following values,

$$\mathrm{Im}(\varphi_1) \in \{0, \pi/2, \pi, 3\pi/2\},$$

and the real component of φ_1 may take $\pm\infty$. When $\mathrm{Re}(\varphi_1) = \pm\infty, 0$ then the state is either on one of the stable or unstable linear subspaces or at the equilibria. Otherwise the imaginary component indicates a partitioning of the saddle subspace into different flows, two of which require $I_1 \geqslant 0$ and the other two require $I_1 \leqslant 0$; we refer to these partitions as quadrants and indicate their type in the figures to follow with $++$, $--$ for the case $I_1 \geqslant 0$, and $+-$ and $-+$ for $I_1 \leqslant 0$.

To demonstrate the effectiveness of the action-angle coordinates (I_j, φ_j) to provide the desirable local orbital element properties of linear dynamical evolution, Figs. 5 and 6 shows the advection of the MC and UT samples using an 18-th order normal form. The erratic behavior of the reference trajectory is expected since the initial condition for it involves $I_1 = \varphi_1 = 0$ and therefore small errors in floating point arithmetic and normal form approximation result in $\mathrm{Re}(\varphi_1)$ easily varying.

Identifying each MC sample with a quadrant, we can examine the flow behavior for each and report on the likelihood that a sample is of each type. This information is shown in Fig. 7. We now proceed to using this partitioning into quadrants to construct our generalized Bernoulli Gauss von Mises (gbGvM) distribution in the next section. The interested

[1]it should be noted that the application of the normal form theory is often a divergent approximation method, and therefore has a finite radius of convergence based on the order of the normal form used

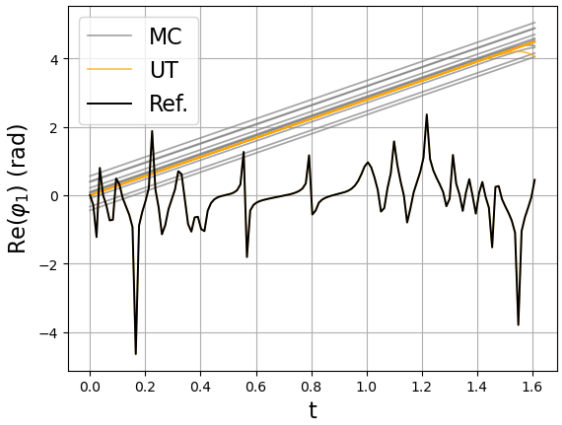

Fig. 6: Evolution of the real component of the angle variable for the saddle term of UT nodes, MC samples, and Lyapunov orbit. Time units are non-dimensionalized, with final time equivalent to 7 days of propagation.

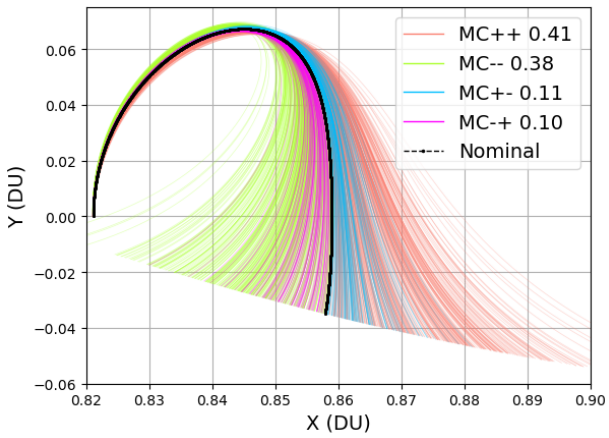

Fig. 7: Evolution of the MC samples and Lyapunov orbit, with identification of quadrant assignment.

reader can see Duarte [28] and Peterson and Scheeres [29] for similar extensions as shown here of Jorba [27] for dynamical systems analysis of the CR3BP.

IV. Generalized Bernoulli Gauss von Mises

Ignoring the singular cases for the action-angle variables (the Lyapunov orbit and the stable and unstable manifolds), the quadrant classification in action-angle coordinates provides an effective categorization by which to create a mixture of four components each of a multivariate distribution on a cylinder space of type $(\mathbb{R}\times S^1)^3$. The weights of each component is assigned based on the likelihood of a sample from a Gaussian in our synodic state representation being associated with a given quadrant. Hence, for the example discussed, the weight vector for the Bernoulli components are $w = (0.41, 0.38, 0.11, 0.1)$. To simplify discussions, and because we are working with a Lyapunov (in-plane) orbit, we drop the out-of-plane aspect of our construction to consider just the saddle-center case.

From Eq. III.3 and the discussion that followed, for each quadrant the action variables take values in the half-space $\overline{\mathbb{R}}_+$. Therefore direct application of a product of Gauss von Mises, each on $\mathbb{R}\times S^1$, is not appropriate. Furthermore, the correlation structure that is critical in the effective definition of the $\mathcal{GVM}$ should be analyzed in the action-angle coordinate system. This has been completed, but for brevity we leave the presentation to a future manuscript. A class of Gaussian derived distributions can be defined on the real-valued half-space. Here we give our first definition using the Folded Normal distribution $\mathcal{F}$, folded at zero, which has the property that as the mean $\mu\to\infty$ and the variance $\sigma^2\to 0$, the folded normal tends to a Gaussian. Hence, in generality we model the uncertainty as,

$$\begin{aligned}
&\text{gb}\mathcal{FVM}(I_1,\text{Re}(\varphi_1),I_2,\varphi_2)\\
&\qquad\equiv\sum_{i=1}^{4} w_i\mathcal{FVM}_i(I_1,\text{Re}(\varphi_1),I_2,\varphi_2)\\
&=\sum_{i=1}^{4} w_i\mathcal{F}_i(I_1;\mu_1,\sigma_1^2)\otimes\mathcal{VM}_i(\text{Re}(\varphi_1);\alpha_1(I_1,I_2),\kappa_1)\\
&\qquad\otimes\mathcal{F}_i(I_2;\mu_2,\sigma_2^2)\otimes\mathcal{VM}_i(\varphi_2;\alpha_2(I_1,I_2),\kappa_2),\quad\text{(IV.1)}
\end{aligned}$$

For the problem under consideration, it is appropriate to consider $\mathcal{F}_2\approx\mathcal{N}_2$ and based on analysis in the action-angle coordinate space, we can approximate $\mathcal{F}_1\approx\mathcal{N}_1$. For this paper, we choose correlation between the von Mises terms and I_1, I_2 as natural extensions of Eq. II.4 and collapse the product of folded normal distributions into a bivariate Gaussian. Hence we arrive at the *generalized Bernoulli Gauss von Mises*,

$$\begin{aligned}
&\text{gb}\mathcal{GVM}(I_1,I_2,\text{Re}(\varphi_1),\varphi_2)\\
&\qquad\equiv\sum_{i=1}^{4} w_i\mathcal{GVM}_i(I_1,I_2,\text{Re}(\varphi_1),\varphi_2)\\
&=\sum_{i=1}^{4} w_i\mathcal{N}_i(I_1,I_2;\mu,P)\otimes\mathcal{VM}_i(\text{Re}(\varphi_1);\alpha_1(I_1,I_2),\kappa_1)\\
&\qquad\otimes\mathcal{VM}_i(\varphi_2;\alpha_2(I_1,I_2),\kappa_2),\quad\text{(IV.2)}
\end{aligned}$$

In this way, all the theory of the $\mathcal{GVM}$ for $\mathbb{R}^5\times S^1$ can be extended to the currently simplified case on $(\mathbb{R}\times S^1)^2$ for us to then judge its efficacy.

A. Application Problem

Returning to our application problem, we show in Figs. 8 and 9 the result of mapping quadrature nodes back from the action-angle coordinate system via the inverse normal form transformation. The MC samples have again been colored according to their quadrant. Although the quadrature nodes appear well placed for the $\dot{x}\times\dot{y}$ plane shown in Fig. 9, their placement in Fig. 8 seems questionable. Yet, advecting these nodes forward to the final epoch displays a remarkably nice fit, as shown in Figs. 10 and 11. This enables an update of the gb$\mathcal{GVM}$ parameters in the action-angle space that well approximates the boomerang deformation behavior.

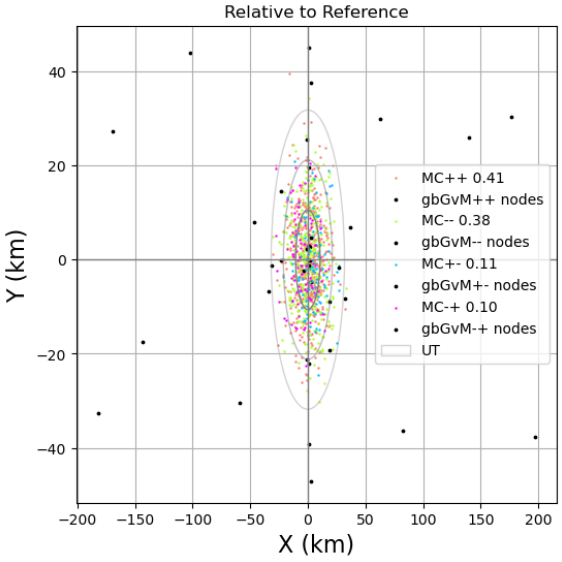

Fig. 8: Quadrature nodes shown against the colorized MC samples according to saddle quadrant classification at the initial epoch in the xy-synodic subspace.

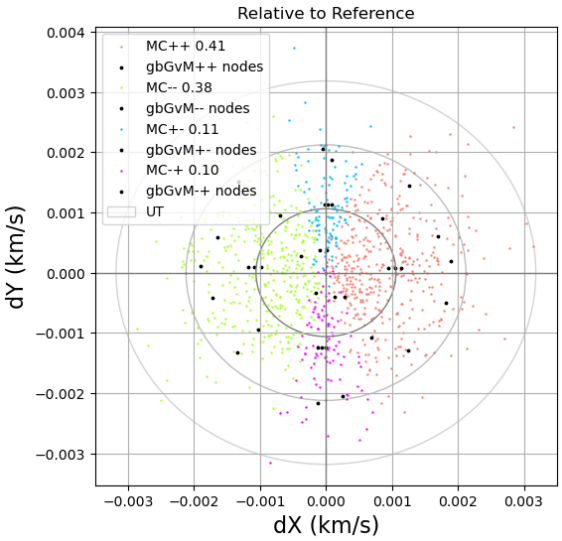

Fig. 9: Quadrature nodes shown against the colorized MC samples according to saddle quadrant classification at the initial epoch in the $\dot{x}\dot{y}$-synodic subspace.

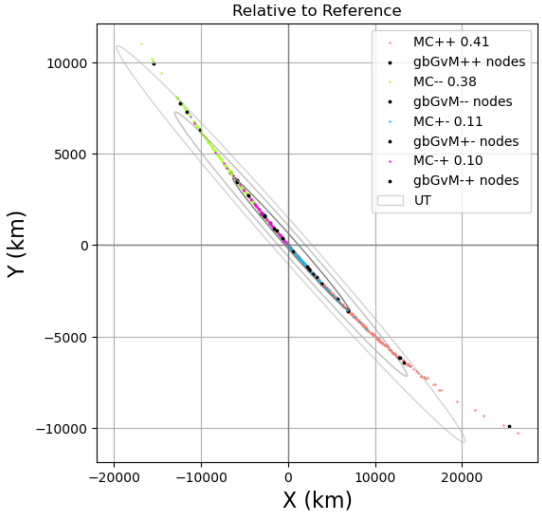

Fig. 10: Advected quadrature nodes shown against the colorized MC samples according to saddle quadrant classification at the final epoch in the xy-synodic subspace.

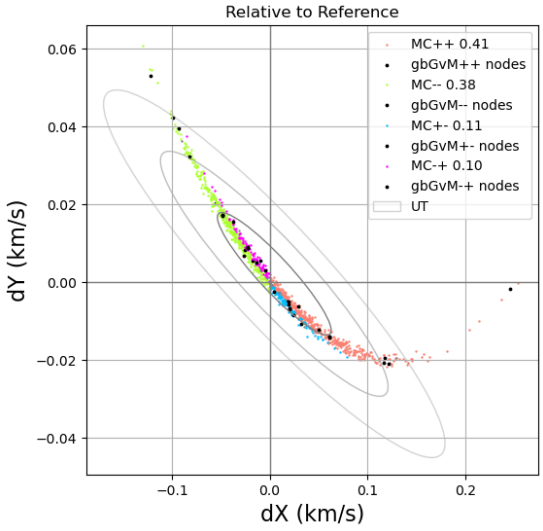

Fig. 11: Advected quadrature nodes shown against the colorized MC samples according to saddle quadrant classification at the final epoch in the $\dot{x}\dot{y}$-synodic subspace.

V. Conclusions

In this paper we motivated the construction of a multivariate distribution defined on a saddle-center space from application problems of SSA to the cislunar domain. Having identified a similar deformation behavior as seen in the two-body problem for Gaussian distributions about libration points, we used the technique of normal form theory, and in particular computational approaches, to generate action-angle coordinates upon which to first construct the generalized Bernoulli Folded von Mises and then argue in approximation to analyze the efficacy of a generalized Bernoulli Gauss von Mises, with inspiration from the Gauss von Mises defined for the two-body problem. There is extensive ongoing work which we are pursuing to better refine and understand this construction. One important aspect is the proper handling and performance of modeling the correlation between components, which is more nuanced than in the two-body case and for which we did not have space here to discuss. A second is the more rigorous construction on half-spaces with the folded normal or similar distribution. There is also the tradeoff of numerical complexity that comes with the order of the normal form transformation.

Although the generation can be done once, the transformation of the quadrature nodes from synodic to action-angle and vice versa requires the evaluation of a power series that grows in computational complexity with the order of the normal form. Lastly, we provide the remark that this technique can be extended to more elaborate dynamical structures, or more directly; the normal form and other parameterization methods can be used directly on the periodic orbits, quasi-periodic ones, and their saddle and center manifolds, as opposed to just the equilibrium points.

REFERENCES

[1] J. T. Horwood and A. B. Poore, "Gauss von mises distribution for improved uncertainty realism in space situational awareness," *SIAM/ASA Journal on Uncertainty Quantification*, vol. 2, no. 1, pp. 276–304, 2014. DOI: 10.1137/130917296.

[2] R. S. Park and D. J. Scheeres, "Nonlinear mapping of gaussian statistics: Theory and applications to spacecraft trajectory design," *Journal of Guidance, Control, and Dynamics*, vol. 29, no. 6, pp. 1367–1375, 2006. DOI: 10.2514/1.20177.

[3] K. Fujimoto and D. J. Scheeres, "Tractable expressions for nonlinearly propagated uncertainties," *Journal of Guidance, Control, and Dynamics*, vol. 38, no. 6, pp. 1146–1151, 2015. DOI: 10.2514/1.G000795.

[4] J. Roa and R. S. Park, "Reduced nonlinear model for orbit uncertainty propagation and estimation," *Journal of Guidance, Control, and Dynamics*, vol. 44, no. 9, pp. 1578–1592, 2021. DOI: 10.2514/1.G005519.

[5] S. Julier, J. Uhlmann, and H. Durrant-Whyte, "A new method for the nonlinear transformation of means and covariances in filters and estimators," *IEEE Transactions on Automatic Control*, vol. 45, no. 3, pp. 477–482, 2000. DOI: 10.1109/9.847726.

[6] S. Julier, "The scaled unscented transformation," in *Proceedings of the 2002 American Control Conference (IEEE Cat. No.CH37301)*, vol. 6, 2002, 4555–4559 vol.6. DOI: 10.1109/ACC.2002.1025369.

[7] S. Julier and J. Uhlmann, "Unscented filtering and nonlinear estimation," *Proceedings of the IEEE*, vol. 92, no. 3, pp. 401–422, 2004. DOI: 10.1109/JPROC.2003.823141.

[8] H. Sorenson and D. Alspach, "Recursive bayesian estimation using gaussian sums," *Automatica*, vol. 7, no. 4, pp. 465–479, 1971, ISSN: 0005-1098. DOI: https://doi.org/10.1016/0005-1098(71)90097-5.

[9] D. Alspach and H. Sorenson, "Nonlinear bayesian estimation using gaussian sum approximations," *IEEE Transactions on Automatic Control*, vol. 17, no. 4, pp. 439–448, 1972. DOI: 10.1109/TAC.1972.1100034.

[10] G. Terejanu, P. Singla, T. Singh, and P. D. Scott, "Uncertainty propagation for nonlinear dynamic systems using gaussian mixture models," *Journal of Guidance, Control, and Dynamics*, vol. 31, no. 6, pp. 1623–1633, 2008. DOI: 10.2514/1.36247.

[11] K. J. DeMars and M. K. Jah, "Probabilistic initial orbit determination using gaussian mixture models," *Journal of Guidance, Control, and Dynamics*, vol. 36, no. 5, pp. 1324–1335, 2013. DOI: 10.2514/1.59844.

[12] K. J. DeMars, R. H. Bishop, and M. K. Jah, "Entropy-based approach for uncertainty propagation of nonlinear dynamical systems," *Journal of Guidance, Control, and Dynamics*, vol. 36, no. 4, pp. 1047–1057, 2013. DOI: 10.2514/1.58987.

[13] B. A. Jones, A. Doostan, and G. H. Born, "Nonlinear propagation of orbit uncertainty using non-intrusive polynomial chaos," *Journal of Guidance, Control, and Dynamics*, vol. 36, no. 2, pp. 430–444, 2013. DOI: 10.2514/1.57599.

[14] D. Xiu and G. E. Karniadakis, "The wiener–askey polynomial chaos for stochastic differential equations," *SIAM Journal on Scientific Computing*, vol. 24, no. 2, pp. 619–644, 2002. DOI: 10.1137/S1064827501387826.

[15] V. Vittaldev, R. P. Russell, and R. Linares, "Spacecraft uncertainty propagation using gaussian mixture models and polynomial chaos expansions," *Journal of Guidance, Control, and Dynamics*, vol. 39, no. 12, pp. 2615–2626, 2016. DOI: 10.2514/1.G001571.

[16] X. Wan and G. E. Karniadakis, "Multi-element generalized polynomial chaos for arbitrary probability measures," *SIAM Journal on Scientific Computing*, vol. 28, no. 3, pp. 901–928, 2006. DOI: 10.1137/050627630.

[17] R. von Mises, "Über die "ganzzahligkeit" der atomgewicht und verwandte fragen," *Physikal*, vol. 19, no. Z, pp. 490–500, 1918.

[18] J. Horwood and A. B. Poore, "Orbital state uncertainty realism," in *Proceedings of the Advanced Maui Optical and Space Surveillance Technologies Conference*, Wailea, HI, 2012, pp. 356–365.

[19] J. T. Horwood, *Methods and systems for updating a predicted location of an object in a multi-dimensional space*, United State Patent: US 8,909,589, Dec. 2014. [Online]. Available: https://s11967.pcdn.co/wp-content/uploads/2019/10/US8909589_p2.pdf.

[20] J. T. Horwood, N. D. Aragon, and A. B. Poore, "Gaussian sum filters for space surveillance: Theory and simulations," *Journal of Guidance, Control, and Dynamics*, vol. 34, no. 6, pp. 1839–1851, 2011. DOI: 10.2514/1.53793.

[21] R. Beeson, "Remarks on the gauss von mises distribution, distributional statistics, and uncertainty realism in space situational awareness," in *AAS/AIAA Astrodynamics Specialist Conference*, 2023.

[22] R. Beeson, A. Sinha, B. Jagannatha, D. Bunce, and D. Carroll, "Dynamically leveraged automated multibody (n) trajectory optimization," in *AAS/AIAA Space Flight Mechanics Conference*, American Astronautical Society, Charlotte, NC, Aug. 2022.

[23] C. C. Chow *et al.*, "Cislunar orbit determination behavior: Processing observations of periodic orbits with gaussian mixture model estimation filters," *The Journal of the Astronautical Sciences*, vol. 69, no. 5, pp. 1477–1492, 2022. DOI: 10.1007/s40295-022-00347-7.

[24] K. R. Meyer and D. Offin, *Introduction to Hamiltonian Dynamical Systems and the N-Body Problem* (Applied Mathematical Sciences), 3rd. New York: Springer Cham, 2017, ISBN: 978-3-319-53691-0. DOI: 10.1007/978-3-319-53691-0.

[25] S. Wiggins, *Introduction to applied nonlinear dynamical systems and chaos*, 2nd. Springer New York, 2003, ISBN: 978-0-387-00177-7. DOI: 10.1007/b97481.

[26] J. Guckenheimer and P. Holmes, *Nonlinear Oscillations, Dynamical Systems, and Bifurcations of Vector Fields* (Applied Mathematical Sciences), Corrected Seventh Printing. Springer, Nov. 2002.

[27] À. Jorba, "A methodology for the numerical computation of normal forms, centre manifolds and first integrals of hamiltonian systems," *Experimental Mathematics*, vol. 8, no. 2, pp. 155–195, 1999. DOI: 10.1080/10586458.1999.10504397.

[28] G. D. Ferreira, "On the dynamics around the collinear points in the sun-jupiter system," Ph.D. dissertation, Universitat de Barcelona, 2019. [Online]. Available: http://hdl.handle.net/10803/668747.

[29] L. T. Peterson and D. J. Scheeres, "Local orbital elements for the circular restricted three-body problem," *Journal of Guidance, Control, and Dynamics*, vol. 46, no. 12, pp. 2275–2289, 2023. DOI: 10.2514/1.G007435.